EFFECT OF ANNEALING TEMPERATURE ON THE STRUCTURAL AND OPTICAL PROPERTIES OF CuI NANOPARTICLES

J. Ruby Jemima[1], R. Vettumperumal[2], D.S. Ivan Jebakumar[3], R. Biju Bennie[3], S. Kalyanaraman[1*]
[1]Research Scholar, Reg No. 9279, PG and Research Department of Physics, Sri Paramakalyani College, Alwarkurichi, Tirunelveli-627 412, Tamil Nadu, India
(Affiliated to Manonmaniam Sundaranar University, Tirunelveli-627 012, Tamil Nadu, India.)
[1*]Principal (Rtd), Sri Paramakalyani College, Alwarkurichi, Tirunelveli-627 412, Tamil Nadu, India
[2]Department of Physics, VV College of Engineering, Tirunelveli-627 657, Tamil Nadu, India.
[3]Department of PG Chemistry, St. John's College, Tirunelveli-627 002, Tamil Nadu, India.

Abstract: Copper iodide (CuI) nanoparticles were synthesized by conventional precipitation method and annealed at four different temperatures to observe the changes in structural, morphological and optical properties. The X-ray diffractograms reveal the existence of zinc blende γ-phase of CuI till 200ºC whereas CuO monoclinic phase begin to emerge in the samples annealed above the temperature. Moreover, the IR interferogram of the samples annealed at temperatures 300ºC and 400ºC indicate the presence of both CuI and CuO in the samples confirming the presence of mixed phase. From the absorbance spectra, the optical bandgap for the samples annealed below 200ºC were calculated which is found to be identical (2.9 eV) and at higher annealing temperature the emerging CuO nanoparticles due to its extensive absorption in visible region obscured the absorption characteristics of CuI. The presence of CuO in the samples annealed above 300ºC is evident from the hump in the absorption spectrum at 675nm. In addition to the blue emission peak of CuI at 430 nm, the defect peak at 684 nm could be observed in the samples annealed above 200ºC. The scanning electron micrographs and EDAX analysis confirms the nucleation of CuO nanoparticles with reduced dimensionality in the CuI matrix at higher annealing temperatures.

Keywords: copper iodide, nanoparticles, copper oxide, annealing, optical bandgap

1. Introduction Copper iodide (CuI), a p-type direct bandgap semiconductor, has attracted the research community for many years because of its wide bandgap, negative spin-orbit splitting and high ionicity [1]. Due to the possibility of tuning hole density with iodine doping, high hole mobility (43.9 $cm^2V^{-1}s^{-1}$) and high transmittance in visible region, CuI is a promising candidate to meet the present need for transparent p-MOS towards the realization of transparent CMOS technology. Attesting to the eco-friendliness of the material, CuI filled single- and multi-walled CNTs have the potential to be used as biocompatible thermometers and also as a source of dietary iodine in table salt. [2-5] CuI shows three polymorphic forms namely (i) γ-CuI, in zinc blende structure, which exists below 370 °C, (ii) β-CuI, in wurtzite structure, is observed between the temperatures 370 to 400 °C and (iii) α-CuI, in rock salt structure, is the high temperature phase which exists above 400 °C [6,7]. As a p-type transparent semiconductor, CuI is an attractive candidate for transparent solid state lighting devices due to high exciton binding energy (62 meV) and also for transparent thermoelectric devices owing to its high thermoelectric conversion efficiency. [8] To synthesize CuI nanostructures, many synthetic techniques have been reported in literature like reactive sputtering, pulsed laser deposition, laser assisted molecular beam deposition, polymer assisted reaction, iodination, wet chemical synthesis and sol-gel technique. [9-15]. In the present investigation, copper iodide nanoparticles were prepared by conventional method and the prepared samples were annealed at four different temperatures 100, 200, 300 and 400 °C and the change in structural and optical properties were studied using appropriate characterization techniques.

2. Experimental Methods

2.1 Materials

All the chemicals used in our experiments were of analytical grade and were used without any further purification. Copper (II) chloride dihydrate ($CuCl_2.2H_2O$) procured from Merck, potassium iodide and Sodium thiosulfate from Himedia were used in our experiments. Deionized water was used throughout the experiment.

2.2 Synthesis of CuI Nanoparticles

In a typical synthesis, 100 mL of 0.5 M reducing agent sodium thiosulphate solution was added in drops to 100 mL of 0.5 M aqueous solution of copper chloride with constant stirring. To the stirred solution, aqueous solution of potassium iodide is added drop by drop and a brown colour precipitate is formed, which was filtered, washed and dried in oven at 60ºC for 4 hours. The samples were annealed in a muffle furnace at four different temperatures of 100, 200, 300 and 400 ºC in ambient atmosphere for 1 hour.

2.3 Characterization Techniques

The X-ray diffractrogram of CuI powders were recorded using XPERT-PRO diffractometer system with CuK_α radiation of wavelength 1.5406 Å in the 2θ range 20-80º. The FTIR spectra for the prepared CuI nanoparticles were recorded using Perkin Elmer spectrometer in the wavenumber range of 400-4000 cm^{-1}. The SEM images were acquired using JEOL JSM-6390 electron microscope at the accelerating voltage of 20kV. UV-visible diffuse reflectance spectra were measured at room temperature employing Agilent Cary 500 UV-VIS-NIR spectrophotometer in the wavelength range of 300 - 1100 nm. Photoluminescence

spectra of the CuI nanoparticles were recorded at room temperature using Shimadzu RF-6000 spectrofluorophotometer at the excitation wavelength of 320 nm in the wavelength range of 350 - 750 nm.

3. Results and Discussion

3.1 Structural Analysis

When X-rays was allowed to incident on a crystalline sample, they are diffracted in a pattern as dictated by the characteristic of the crystal structure. The Bragg's law imposes the condition for constructive interference to obtain XRD patterns and the powder diffraction patterns of the prepared samples are shown in the Fig. 1.

The peaks in the XRD pattern of nanoparticles are in good agreement with the reported standards (JCPDS card no. 76-0207) and the peaks at 2θ values 25.5, 29.5, 42.2, 50, 61.2, 67.4, 69.4 and 77.1 could be indexed to the (111), (200), (220), (311), (222), (400), (331) and (420) planes of γ-CuI for the samples annealed at 100 and 200ºC which is in accordance with that of the pure phase of copper iodide in zinc blende crystal structure.

The XRD diffractogram of the samples annealed at 300 and 400ºC shows the reflections for monoclinic copper oxide along with those obtained for copper iodide. The copper oxide peaks begins to emerge around 300 ºC and dominates in the sample annealed at 400ºC. This agrees well with the standard values reported in the literature (JCPDS card no. 89-2531) and it shows monoclinic structure of CuO. The additional peaks appear in the diffractogram of samples annealed above 300 ºC at 2θ values 32.5, 35.57, 38.78, 46.5, 48.8, 53.5, 58.3, 61.5, 66.3, 68.10 could be indexed to (110), (002) & (-111), (200) & (111), (-112), (-202), (020), (202), (-113), (022), and (220) planes of CuO. The crystallite size of CuI was determined using the Scherrer formula as given by,

$$D = k \lambda / \beta \cos \theta$$

where k = 0.9 is the correction factor for particle shape, β is the full width at half maximum (FWHM), λ is the wavelength of X-rays and θ is the angle of incidence [16]. The average crystallite size of CuI nanoparticles are 54 nm, 45 nm, 43 nm and 42 nm for the samples annealed at 100, 200, 300 and 400 ºC respectively. The decrease in crystallite size with increasing annealing temperature could be attributed to the nucleation of monoclinic CuO in zinc blende CuI matrix with small crystallite size than that of CuI.

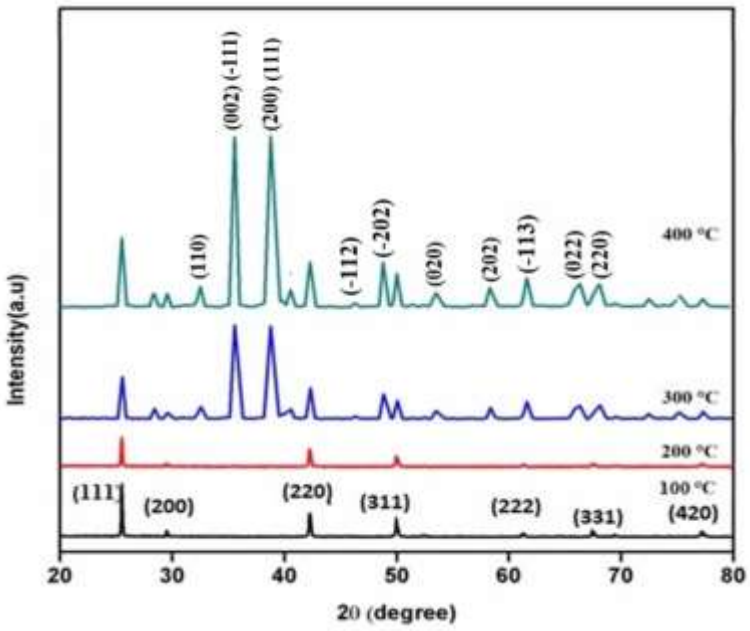

Fig.1. Powder XRD patterns of pure CuI and CuI-CuO mixed phase nanoparticles at different annealing temperatures

3.2 Functional Group Analysis

FT-IR technique is one of the most essential and extensively used spectroscopic techniques to identify the functional groups, to determine the internal structure of the molecules and to understand the nature of chemical environment in the given compound. Since the X-ray diffraction patterns of the CuI samples annealed at 100 and 200 ºC is found to be the same, the IR interferogram of both the samples were also similar.

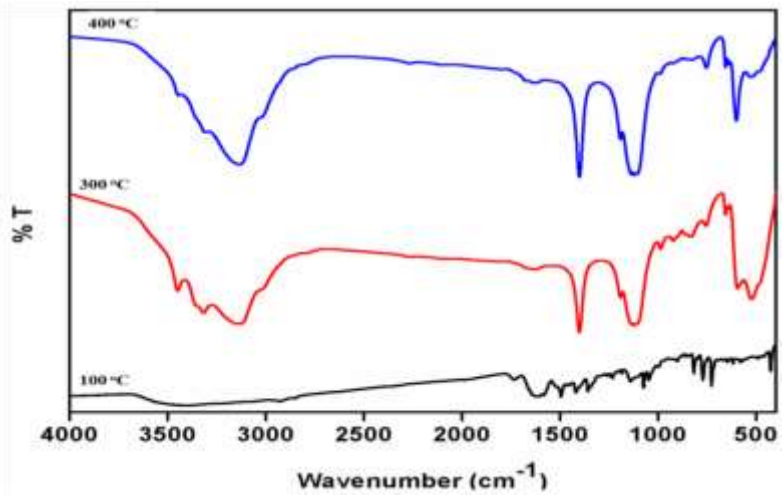

Fig 2. FT-IR spectra of pure CuI and CuI-CuO mixed phase nanoparticles at different temperatures

The recorded IR interferogram for the samples annealed at 100, 300 and 400 ºC are displayed in Fig 2. The bands in the range of 3450-3100 cm^{-1} correspond to the OH stretching vibrations which may be due to the adsorbed H_2O molecules on the CuI-CuO samples. The bands were absent in pure CuI sample due to its hydrophobic nature which is further supported by the high contact angle for water [17]. The assignment of the peak observed in the region of 522 cm^{-1} is designated to Cu-I stretching vibration [18]. The bands corresponding to copper oxide are found in the range of 500-700 cm^{-1} [19], which confirm the formation of CuI/CuO nanocomposites at higher annealing temperatures.

3.3 Morphological Analysis

The SEM images acquired for the CuI samples annealed at different temperatures are displayed in Fig. 3 and the significant change in morphology could be observed when the samples annealed at higher temperature. The SEM micrograph of CuI annealed at 100ºC shows the triangular morphology of the sample as reported in the literature [20, 21]. The EDAX microanalysis of CuI-CuO mixed phase nanostructures (in fig 3 (d)) reveals the presence of elements Cu and I as that for CuI nanostructures and in addition it also showed the presence of oxygen.

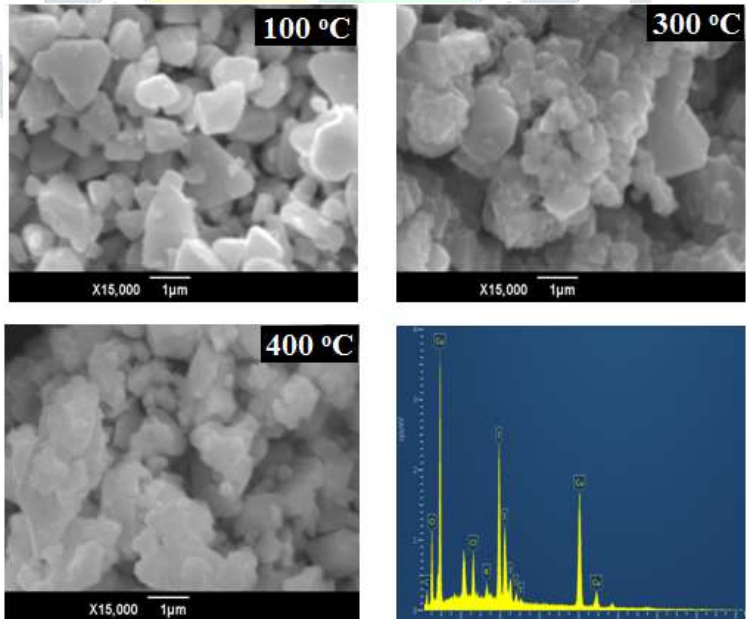

Fig 3. SEM micrographs of the samples annealed at a) 100 ºC, b) 300 ºC and c) 400 ºC

d) EDAX spectrum of CuI-CuO mixed phase nanostructures.

3.4 Absorbance and Emission Spectral Analysis

UV-visible absorption spectra of the samples were recorded in the range of 200-900 nm and are shown in the Fig 4(a-d). Fig. 4a shows absorption features at 320 nm and 410 nm, which could be attributed to the excitation of electrons to the conduction band from sublevels and interband excitonic absorptions respectively. But in the samples annealed at 300 and 400 ºC (Fig. 4c and

4d), there exists an additional hump in the visible region around 675 nm which is ascribed to the absorption of CuO nanoparticles [22] present in the sample.

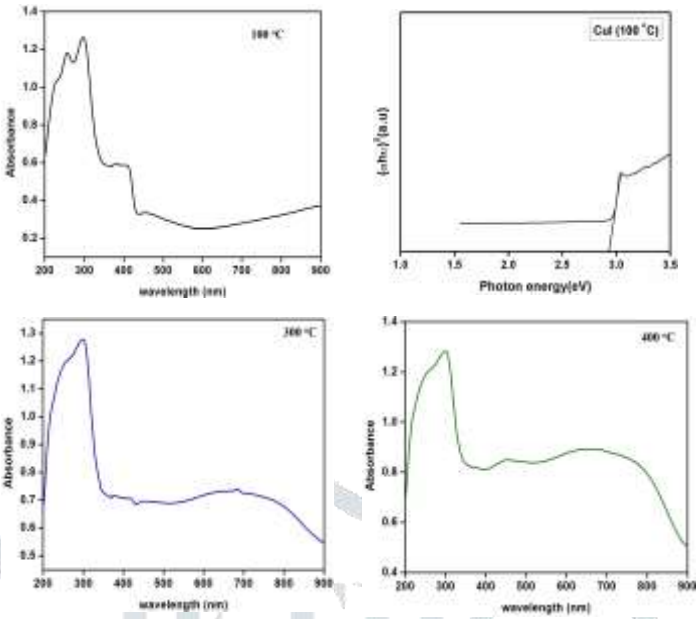

Fig 4. (a), (c), (d) UV-vis spectra of the samples annealed at 100 ºC, 300ºC and 400ºC
(b) Variation of $(\alpha h\nu)^2$ with photon energy for CuI nanoparticles annealed at 100 ºC

The optical bandgap E_g is estimated using the formula,

$$(\alpha h\nu)^2 = A(h\nu - E_g)$$

where A is a constant and hν is the photon energy. From the plot of $(\alpha h\nu)^2$ *vs* hν, the bandgap is determined by drawing a tangent to the linear portion of the curve and extrapolating the same to the photon energy (x-axis) at αhν=0. Fig. 4(b) shows the Tauc plot for the CuI nanoparticles annealed at 100 ºC, where the bandgap was found to be 2.9 eV and is in accordance with the values reported earlier for CuI nanoparticles [23]. But for samples annealed at 300 and 400ºC, the absorption edge were observed at 364 nm and 354 nm respectively. The absorption features of the CuI nanoparticles are masked by the absorption spectrum of the resulting CuO formed during annealing above 400ºC due to the higher absorption coefficient of CuO [24, 25] compared to CuI at the visible region.

The photoluminescence (PL) spectra of the samples annealed at four different temperatures are displayed in Fig. 6. The photoluminescence spectra of CuI sample annealed at 100 ºC and 200 ºC were found to be identical. Photoluminescence of CuI sample annealed at 100 ºC shows a narrow blue emission peak centered at 430 nm [26, 27] while the samples annealed at 300 and 400 ºC show a broad and asymmetric emission peak around 455 nm accompanied by the weak emission at 684 nm. The emission peaks at 430 nm and 455 nm originates from band edge emission of CuI nanoparticles whereas the red luminescence at 684 nm could be due to defect emission as a result of the iodine vacancies [28] formed in CuI samples with increase in annealing temperature. No emission peaks from CuO was observed in the spectrum due to apparently poor photoluminescence efficiency of CuO compared to CuI.

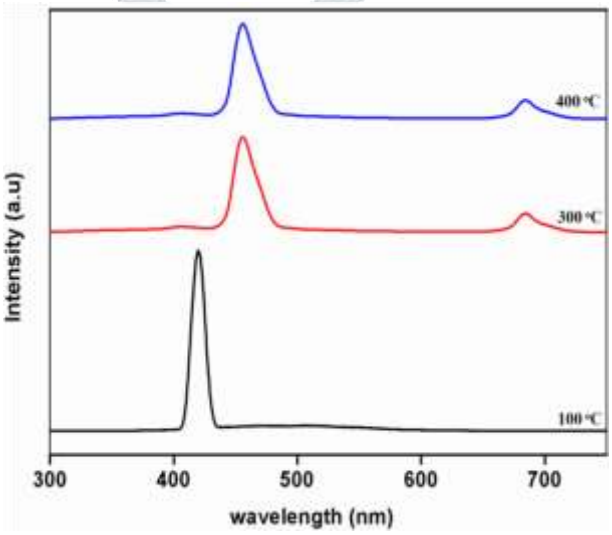

Fig 5. Photoluminescence Spectrum for the samples annealed at 100 ºC, 300 ºC and 400 ºC.

4. Conclusion

The nanoparticles of pure CuI and CuI/CuO mixed phase have been prepared by precipitation method and annealed at four different temperatures. The structural and optical properties of annealed nanoparticles have been examined by various characterization techniques. The XRD patterns show pure γ-CuI phase at 100 and 200 ºC while the emergence of additional peaks at higher annealing temperatures represents the formation of monoclinic CuO phase along with γ-CuI. The presence of CuO in the sample annealed at 300 and 400 ºC is further confirmed from FT-IR spectral studies and the hydrophobicity of the samples was found to decrease with the formation of mixed phase. CuI and CuI/CuO nanoparticles morphology were studied from SEM micrographs which show the nucleation of CuO nanoparticles with reduction of particle size in the samples annealed at higher temperature. The bandgap values from UV-Vis spectra for the samples annealed at 100 ºC matches well with pure CuI and the absorption spectra of CuI nanoparticles were masked by the absorption of the CuO particle formed at higher annealing temperature. The photoluminescence spectra shows optical emission from pure CuI phase at lower annealing temperatures below 200 ºC whereas additional emission peak due to defect emission was also observed in mixed CuI-CuO phase samples that were annealed at higher annealing temperatures.

Acknowledgement

The authors are thankful to STIC (Cochin), Department of Physics (Alagappa University, Karaikudi), Department of Chemistry (St. Joseph's College, Trichy) and Department of Chemistry (VOC College, Tuticorin) for the characterization facilities.

References:

1. Naoomi Yamada, Ryuichiro Ino, Yoshihiko Ninomiya, *Chem. Mater*., **28** (2016) 4971.
2. S. Gao, Z. Li, .X. Jia, K. Jiang, H. Zeng, *Green Chem*. **12** (2010) 1442.
3. A. Klapars, S. L. Buchwald, *J. Am. Chem. Soc*. **124** (2002) 14844.
4. C. H. B. Ng, W. Y. Fan, *J. Phys. Chem C*, **111** (2007) 9166.
5. Y. Y. Xu, D. R. Chen, X. L. Jiao, *Mater. Lett*. **63** (2009) 1859.
6. Marius Grundmann, Friedrich-Leonhard Schein, Michael Lorenz, Tammoöntgen, Jörg Lenzner, and Holger von Wenckstern, *Phys. stat. sol.* (a) **210** (2013), 1671.
7. J. B. Boyce, T. M. Hayes, J. C. Mikkelsen, *Phys. Rev. B*, **23** (1981) 2876.
8. Bruno Miguel, Morais Faustino, Diogo Gomes, Jaime Faria, Taneli Juntunen, Guilherme Gaspar, Catarina Bianchi, António Almeida, Ana Marques, Ilkka Tittonen, Isabel Ferreira, *Scientific Reports*, **8** (2018) 6867.
9. W. M. K. P. Wijekoon, M. Y. M. Lyktey, P. N. Prasad, J. F. Garvey, *J. Appl. Phys*. **74** (1993) 5767.
10. V. Y. Bokshis, A.Y. Fedutic, G. P. Shevchnko, *Colloid Journal*, **66** (2004)25.
11. K. Reichld, M. J. Florian, *Cryst. Growth*, **44** (1978) 507.
12. P. M. Sirimanne, M. Rusop, T. Shirata, T. Soga, T. Jimbo, *Mater. Chem. Phys*., **80** (2003) 461.
13. M. Ying, J. Z. Xu, S. Xu, J. J. Zhu, H. Y. Chen, *Inorg. Chem. Comm*. **7** (2004) 628.
14. Y. Xu, D. Chen, X. Jiao, L. Ba, *J. Phys. Chem. C*, **111** (2007) 6.
15. Meng Lr, R. Mo, H. Zhou, G. Wang, W. Chen, D. Wang, *Cryst. Growth Des*., **10** (2010) 3387.
16. B. D. Cullity, Elements of X-ray Diffraction, Addison Wesley, 1977, pp. 81.
17. R. N. Bulakhe, N. M. Shinde, R. D. Thorat, S. S. Nikam, C. D. Lokhande, *Curr. Appl. Phys.*, **13** (2013) 1661.
18. R. Hammad Humud, *J. Chem. Pharm. Res*., **9** (2017) 31-36.
19. Vinod Vellora Thekkaepadil, Miroslav Cernik, *Inter. J. Nano Med*., **8** (2013) 889.
20. C. Yang, M. Kneib, F. Schein, M. Lorenz, M. Grundmann, *Scientific Reports* 21937 **6**(2016), 1-8.
21. B. Mahdi, N. Ali, *Romanian Journal of Biochemistry*, **51** (2014) 101-107.
22. Jiji Koshy, M. Soosen Samuel, Anoop Chandran, K. C. George, AIP Conf. Proc., 1391, **576** (2011).
23. W. Sekkal, A. Zaoui, *Physica B: Condensed Matter*., **315** (2002) 201.
24. Chang Yang, Max Kneiβ, Michael Lorenz, and Marius Grundmann, PNAS **113** (2016), 12929.
25. Anagh Bhaumik, Austin M. Shearin, Rishi Patela, Kartik Ghosh, *Phys. Chem. Chem. Phys*., **16** (2014) 11054.
26. S. Amrut Lanje, *Adv. Appl. Sci. Res*., **1** (2010) 36.
27. U. Kester Ighodalo, *Mater. Res. Bull*., **94** (2017) 528.
28. Pan Gao, Mu Gu, Xiao-Lin Liu, Bo Liu, Shi-Ming Huang, *Appl. Phys. Lett*., **95** (2009), 221904.